Hindawi
Geofluids
Volume 2021, Article ID 5568336, 12 pages
https://doi.org/10.1155/2021/5568336

Research Article

The Effect of Rheology of Viscoelastic Polymer on Pressure Transient Response in Near-Wellbore Regions

Jia Zhang,[1] **Shiqing Cheng**,[1] **Jie Zhan**,[2] **and Qi Han**[3]

[1]*State Key Laboratory of Petroleum Resources and Prospecting, China University of Petroleum, Beijing 102249, China*
[2]*School of Petroleum Engineering, Xi'an Shiyou University, Xi'an 710065, China*
[3]*Exploration and Development Research Institute, PetroChina Huabei Oilfeld Company, 062552, China*

Correspondence should be addressed to Jia Zhang; 2017312042@student.cup.edu.cn and Shiqing Cheng; chengsq973@163.com

Received 24 February 2021; Accepted 20 May 2021; Published 8 June 2021

Academic Editor: Yonghui Wu

Viscoelastic polymer solution shows shear thinning behavior at low shear rates and shear thickening behavior at high shear rates in reservoirs. However, models that ignored shear thickening behavior were commonly employed to interpret transient pressure data derived from tested wells in viscoelastic polymer flooding systems; although, viscoelastic polymer solutions show shear thickening behavior in the near-wellbore region due to high shear rate. To better characterize the oilfield with pressure transient analysis in viscoelastic polymer flooding systems, we developed a numerical model that takes into account both shear thinning behavior and shear thickening behavior. A finite volume method was employed to discretize partially differential flow equations in a hybrid grid system including PEBI mesh and Cartesian grid, and the Newton-Raphson method was used to solve the fully implicit nonlinear system. To illustrate the significance of our model, we compared our model with a model that ignores the shear thickening behavior by graphing their solutions on log-log plots. In the flow regime of near-wellbore damage, the pressure derivative computed by our model is distinctly larger than that computed by the model ignoring shear thickening behavior. Furthermore, the effect of shear thickening behavior on pressure derivative differs from that of near-wellbore damage. We then investigated the influence of shear thickening behavior on pressure derivative with different polymer injection rates, injection rates, and permeabilities. The results can provide a benchmark to better estimate near-wellbore damage in viscoelastic polymer flooding systems. Besides, we demonstrated the applicability and accuracy of our model by interpreting transient pressure data from a field case in an oilfield with viscoelastic polymer flooding treatments.

1. Introduction

Crude oil plays an important role in contributing to the world's energy consumption. Polymer flooding is widely employed in oilfields as a mature and economic process by increasing sweep efficiency in oil development [1–5]. In the design and adjustment of the polymer flooding process, basic information of an oilfield is the key to success. Pressure transient analysis is an important method to characterize reservoirs [6–12], which can provide valuable information including permeability, degree of near-wellbore damage (skin factor) [13–20], and wellbore storage constant.

To expand pressure transient analysis to polymer flooding, we must overcome several challenges. The most important one is that polymer solution shows either or both shear thinning and shear thickening in porous media. More specifically, shear thinning behavior is that the viscosity of the viscous polymer solution decreases with the shear rate [21–24]. However, for viscoelastic polymer solutions, the viscosity decreases with the shear rate at low shear rates and increases when the shear rate increases at high shear rates [25–28]. Due to the above non-Newtonian nature of the polymer, the well test model used for the water flooding system is no longer suitable for the polymer flooding system.

For the viscous polymer, a simplified single-phase model solved by the finite difference method was presented by Poollen and Jargon [29] to investigate the pressure transient behavior of a field test. Then, Ikoku and Ramey [30] and Odeh and Yang [31] developed analytical solutions of single-phase models to introduce new methods of pressure transient analysis for the viscous polymer solution. Further, Lund [32] expanded the pressure transient theory for the non-Newtonian shear-thinning fluids into composite reservoirs, in which he assumed a radial flow system consisting of non-Newtonian and Newtonian fluids with a single-phase model. To model the flow of the shear-thinning polymer solution in a vertically fractured well system, Murtha and Ertekin [33] developed a numerical simulator for single-phase flow. On this basis, Vongvuthipornchai and Raghavan [34] analyzed the pressure transient behavior of fractured wells after the injection of the viscous polymer solution. Mahani et al. [35] combined numerical simulations and analytical pressure transient computations to infer the in situ polymer rheology in a polymer flooding system. Kamal et al. [36] developed analytical solutions of single-phase well test models combining the non-Newtonian shear-thinning fluids and the multicomposite reservoir, which can be used to obtain reservoir properties in various banks and the location of the flood front. However, the above models ignored the effect of concentration gradients and saturation gradients on the pressure transient behavior during polymer flooding. To fill this gap, Zhang and Yao [37] proposed a numerical model for two-phase flow to investigate the transient pressure behavior of wells after the injection of the viscous polymer solution. Jia et al. [38] proposed a numerical model of two-phase flow considering the shear-thinning behavior of polymer solutions to study pressure transient response in polymer flooding systems.

Though the above models are satisfying in the well test interpretation for the viscous polymer flooding, the influence of shear thickening behavior on pressure transient behavior is ignored in viscoelastic polymer flooding systems. To fill this gap, Yang et al. [39] and Xie et al. [40] investigated the effect of shear-thickening behavior on the pressure response of injection wells during polymer injection with single-phase models. Furthermore, Ma and McClure [41] discovered that the shear thickening behavior influences the early part of the shut-in pressure of polymer injection wells in a viscoelastic polymer flooding system with a single-phase model. However, they did not further analyze the impact of shear thickening behavior on transient pressure response in well test interpretation.

Therefore, the impact of shear thickening behavior on the pressure transient response still needs to be discussed in well test interpretation. Ignoring the impact of shear thickening behavior can lead to errors in the diagnosis and interpretation of the transient pressure data, which are obtained from the falloff tests in viscoelastic polymer flooding systems. To solve this problem, a numerical model for two-phase is urgently needed to investigate the transient pressure behavior of falloff tests in viscoelastic polymer flooding systems.

The objective of this paper is to better characterize the oilfield with pressure transient analysis by investigating the effect of shear thickening behavior on the pressure transient response of falloff tests in viscoelastic polymer flooding systems. Because partially hydrolyzed polyacrylamide (HPAM) is the most commonly employed viscoelastic polymer in polymer flooding, we analyzed the effect of shear thickening behavior of HPAM on the pressure transient response with a developed two-phase numerical model. To validate the applicability and accuracy of our model, we interpreted the transient pressure data obtained from a polymer injection well in an oilfield.

2. Model Development

To investigate the transient pressure response in a viscoelastic polymer flooding system, we developed a numerical model for two-phase flow. To solve our model more efficiently, the flow equations are discretized with a finite volume method in a hybrid grid system including PEBI mesh and Cartesian grid. Then, we applied a fully implicit Newton-Raphson method to solve the discrete flow equations.

2.1. Model Description. To model the flow of the partially hydrolyzed polyacrylamide (HPAM), water, and oil in polymer flooding systems, the following basic assumptions are made:

(1) The shear thickening behavior, shear thinning behavior, convection, and adsorption of the HPAM are considered. Diffusion and dispersion are ignored due to their insignificant effect on the pressure transient response. We also consider the permeability reduction of the aqueous phase derived from the polymer adsorption and the inaccessible pore volume due to the large molecular size and flexible structure of the HPAM

(2) The reservoir is isotropic and isothermal; the initial pressure, initial water saturation, and initial polymer concentration are distributed uniformly in the reservoir. The exterior boundary of the reservoir is closed

(3) The reservoir fluids contain water and oil. The HPAM dissolves in the aqueous phase, and so we consider that the effective viscosity of the aqueous phase equals to the viscosity of polymer solution. No chemical reaction takes place during polymer flooding

(4) The relative permeability of the oil phase and aqueous phase is considered. The capillary pressure is neglected because of its small impact on the transient pressure behavior in polymer flooding systems

(5) The flow of the oil phase and aqueous phase in the reservoir follows the Darcy's law. Fluids and rocks are kind of compressible

2.2. Mathematical Model. On the basis of the above assumptions, we propose the partially differential flow equations of the oil, water, and polymer.

$$\frac{\partial}{\partial t}(\phi b_\alpha S_\alpha)+\nabla\cdot(b_\alpha v_\alpha)-Q_\alpha=0,\ \alpha=\{o,w\}, \tag{1}$$

$$\frac{\partial}{\partial t}\left[\phi f_p b_w\left(S_w C_p+\hat{C}_p\right)\right]+\nabla\cdot\left(b_w v_w C_p\right)-Q_w C_p=0, \tag{2}$$

where b_α is the reciprocal of the oil or aqueous formation volume factor, f_p is the ratio of the accessible pore volume to the pore volume of reservoir rocks, C_p is the polymer concentration of the aqueous phase, and $\hat{C}_p$ is the adsorbed concentration of polymer on the rock surface.

Given that the relative permeability and permeability reduction are considered, the velocities of oil and aqueous can be replaced by the following equations.

$$\begin{aligned} v_o &= -\frac{Kk_{ro}}{\mu_o}(\nabla p_o),\\ v_w &= -\frac{Kk_{rw}}{\mu_{\text{weff}}R_k}(\nabla p_w), \end{aligned} \tag{3}$$

where μ_{weff} is the effective viscosity of aqueous phase considering the dissolved polymer, and R_k is the permeability reduction factor for aqueous phase.

The adsorbed concentration of polymer ($\hat{C}_p$) in Equation (2) is expressed by the Langmuir adsorption equation.

$$\hat{C}_p=\frac{\hat{C}_{p\,\max}b_p C_p}{1+b_p C_p}, \tag{4}$$

where $\hat{C}_{p\,\max}$ is the saturated adsorbed concentration of polymer, and b_p is the constant parameter.

The permeability reduction factor for the aqueous phase is described by Hou et al. [42].

$$R_k=1+\frac{(R_{k\,\max}-1)b_p C_p}{1+b_p C_p}, \tag{5}$$

where $R_{k\,\max}$ is the maximum permeability reduction factor.

Although the rates of tested wells are known parameters in well tests, we still require to compute oil or aqueous flow rates of wellbores. Furthermore, the wellbore storage is taken into account in our model for pressure transient analysis, which is ignored in the model of reservoir simulation.

$$Q_s=\sum(Q_w+Q_o),$$

$$Q_\alpha=\frac{2\pi K\lambda_\alpha h b_\alpha}{(\ln(r_e/r_w)+S)}\left(p_{wf}-p_\alpha\right)+Cb_\alpha\frac{dp_{wf}}{dt},\qquad \begin{cases}\lambda_o=\dfrac{k_{ro}}{\mu_o}\\ \lambda_w=\dfrac{k_{rw}}{\mu_{\text{weff}}R_k}\end{cases}. \tag{6}$$

To calculate the effective viscosity of the aqueous phase in viscoelastic polymer flooding systems, we employ a unified viscosity model of polymer solutions proposed by Delshad et al. [43]. The model can characterize the shear thinning behavior and shear thickening behavior of the partially hydrolyzed polyacrylamide (HPAM) solution. The great advantage of Delshad's model is that it only requires bulk rheology data and petrophysical information of the porous media.

$$\begin{aligned} \mu_{weff}=\mu_w+\left(\mu_p^0-\mu_w\right)\left[1+(\lambda_1\gamma)^2\right]^{\frac{n_1-1}{2}}\\ +\mu_{\max}\left\{1-\exp\left[-(\lambda_2\tau_r\gamma)^{n_2-1}\right]\right\}. \end{aligned} \tag{7}$$

If the shear thickening behavior of polymer solutions is neglected, Equation (7) can be simplified into the following expression.

$$\mu_{\text{weff}}=\mu_w+\left(\mu_p^0-\mu_w\right)\left[1+(\lambda_1\gamma)^2\right]^{\frac{n_1-1}{2}}, \tag{8}$$

where γ is the shear rate of the polymer solution, μ_p^0 is the viscosity of the polymer solution at zero shear rate, and n_1, n_2, and λ_2 are empirical constants.

In the above viscosity model, λ_1, $\mu_{\max}$, and τ_r are functions of the polymer concentration.

$$\begin{aligned} \lambda&=\beta_1\exp\left(\beta_2 C_p\right),\\ \mu_{\max}&=\mu_w\left[1+\left(A_{p1}C_p+A_{p2}C_p^2\right)C_{\text{sep}}^{sp}\right],\\ \tau_r&=\tau_0+\tau_1 C_p, \end{aligned} \tag{9}$$

where β_1, β_2, A_{p1}, A_{p2}, τ_0, and τ_1 are constant parameters. C_{sep} is effective salinity, and sp is constant parameters.

The zero shear viscosity (μ_p^0) in Equation (7) and Equation (8) is a function of the polymer concentration (C_p) and effective salinity (C_{sep}).

$$\mu_p^0=\mu_w\left[1+\left(A_1C_p+A_2C_p^2+A_3C_p^3\right)C_{\text{sep}}^{sp}\right], \tag{10}$$

where A_1, A_2, and A_3 are input constants.

To illustrate the influence of shear thickening behavior on polymer viscosity, we compute the viscosity of polymer solution considering or ignoring the shear thickening behavior (Figure 1). The values of the input parameters for calculating the apparent viscosity are listed in Table 1.

According to Equation (7), we can calculate the viscosity of the HPAM solution as a function of the shear rate for different polymer concentrations, as illustrated in Figure 2.

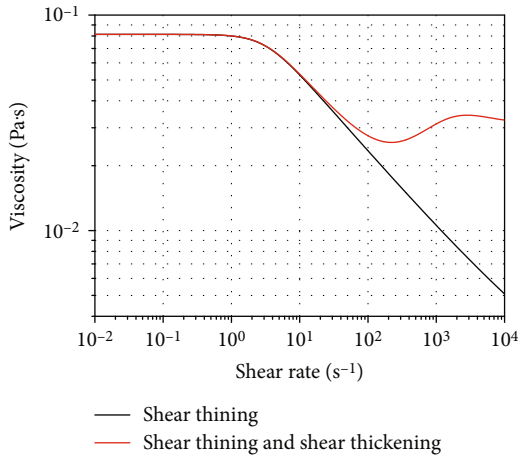

Figure 1: The viscosity of the viscoelastic polymer solution considering shear thickening behavior and shear thinning behavior and the viscosity of the polymer solution that ignores shear thickening behavior.

Table 1: The input constants for calculating the apparent viscosity of the HPAM solution.

Parameters	Values	Parameters	Values
μ_w, Pa·s	0.00099	τ_0, unitless	0.005989
n_1, unitless	0.63	τ_1, unitless	0.1562
n_2, unitless	1.94	C_{sep}, kg/m^3	0.33496
λ_2, unitless	0.0088	sp, unitless	0.7
β_1, unitless	0.0172	A_1, unitless	82.53
β_2, unitless	2.903	A_2, unitless	51.14
A_{p1}, unitless	53.387	A_3, unitless	60.07
A_{p2}, unitless	4.152		

The shear rate (γ) in Equation (7) and Equation (8) is proposed by Wang [44, 45] based on the model of single-phase flow presented by Cannella et al. [46].

$$\gamma = \frac{4|v_w|}{\sqrt{8C' K k_{rw}\phi/R_k}}\left[\frac{(3n+1)}{4n}\right]^{\left(\frac{n}{n-1}\right)}, \tag{11}$$

where C' and n are constant input parameters.

2.3. Differentiation and Solution. To solve the partially differential flow equations, we discretize them in a hybrid grid system including PEBI mesh and Cartesian grid first (Figure 3). The near-well zone consists of refined PEBI meshes because the shear thickening behavior of polymer solutions occurs mainly in this zone due to high shear rate. To reduce computation time, the Cartesian grids of large size are distributed far away from the wellbore. In the hybrid system, each grid or mesh contains cell (c), face (f), and node.

In unstructured grids, the finite volume method [47] is easily formulated, and thus we employ it to discretize the above partially differential flow equations. To make discrete equations easy to comprehend, we employ the discrete operators div and grad for the divergence and gradient operators, respectively [48, 49].

Thus, the flux passing through the face f can be written as

$$\mathbf{q}[f] = -\mathbf{T}[f]\ \text{grad}\ (\mathbf{p})[f], \tag{12}$$

where q is the array of discrete fluxes, T is the array of discrete transmissibilities through faces, and p is the array of the pressure gradient.

Following the above discrete operators, we discretize Equations (1) and 2 with upstream weighting

$$\begin{aligned}\mathbf{R}_\alpha^{n+1,l} = \mathbf{V}[c]&\frac{(\boldsymbol{\phi}[c]\mathbf{b}_\alpha[c]\mathbf{S}_\alpha[c])^{n+1,l} - (\boldsymbol{\phi}[c]\mathbf{b}_\alpha[c]\mathbf{S}_\alpha[c])^n}{\Delta t^{n+1}}\\ &+\text{div}(\mathbf{b}_\alpha[f]\mathbf{v}_\alpha[f])^{n+1,l} - (\mathbf{Q}_\alpha[c])^{n+1,l} = 0,\end{aligned} \tag{13}$$

$$\begin{aligned}\mathbf{R}_p^{n+1,l} = \mathbf{V}[c]&\frac{\left\{\boldsymbol{\phi}[c]f_p\mathbf{b}_w[c]\left(\mathbf{S}_w[c]\mathbf{C}_p[c] + \widehat{\mathbf{C}}_p[c]\right)\right\}^{n+1,l} - \left\{\boldsymbol{\phi}[c]f_p\mathbf{b}_w[c]\left(\mathbf{S}_w[c]\mathbf{C}_p[c] + \widehat{\mathbf{C}}_p[c]\right)\right\}^{n}}{\Delta t^{n+1}}\\ &+\text{div}\left(\mathbf{b}_w[f]\mathbf{v}_w[f]\mathbf{C}_p[f]\right)^{n+1,l} - \left(\mathbf{Q}_w[c]\mathbf{C}_p[c]\right)^{n+1,l} = 0.\end{aligned} \tag{14}$$

Note that we denote arrays of discrete variables with boldfaced letters in the above discrete equations. In Equations (13) and 14, $v_\alpha[f]$ can be substituted by the following expression.

$$\mathbf{v}_\alpha[f] = -\mathbf{T}[f]\boldsymbol{\lambda}_\alpha[f]\{\text{grad}\ (\mathbf{p}_\alpha)[f]\} \tag{15}$$

Then, we discretize the well equation.

$$\mathbf{R}_q^{n+1.l} = (\mathbf{Q}_s[c])^{n+1} - \sum_j (\mathbf{Q}_\alpha[c])^{n+1,l} = 0. \tag{16}$$

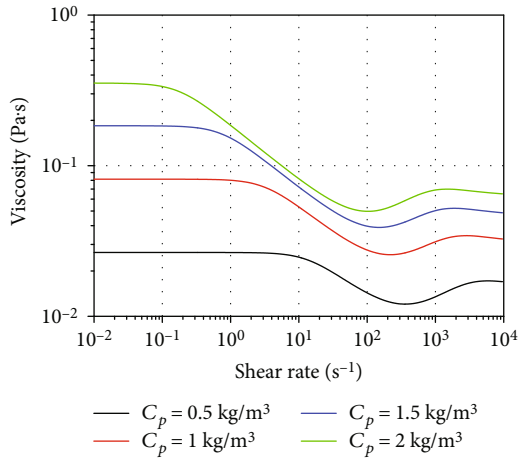

Figure 2: The viscosity of the partially hydrolyzed polyacrylamide (HPAM) solution as a function of the shear rate for different polymer concentrations.

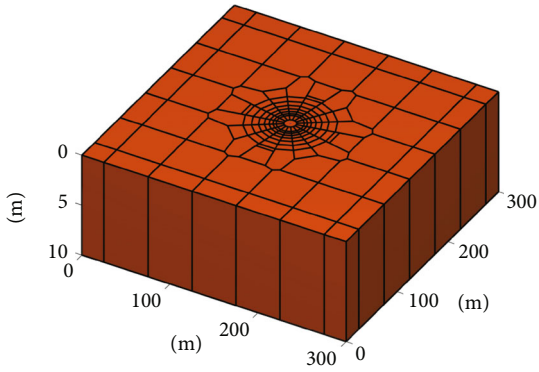

Figure 3: A hybrid grid system including PEBI mesh and Cartesian grid.

The flow rate of the oil/aqueous phase in Equation (16) can be written as [49]

$$\mathbf{Q}_{\alpha}^{n+1,l} = \left\{\frac{2\pi\lambda_{\alpha}[c]h\mathbf{b}_{\alpha}[c]}{\ln(r_e/r_w)+S}\right\}^{n+1,l}\left(\mathbf{p}_{wf}[c]-\mathbf{p}_{\alpha}[c]\right)^{n+1,l} + \{C\mathbf{b}_{\alpha}[c]\}^{n+1,l}\frac{\mathbf{p}_{wf}^{n+1,l}[c]-\mathbf{p}_{wf}^{n}[c]}{\Delta t^{n+1}}. \quad (17)$$

Coupling with Equations (13)-(17), we obtain

$$\mathbf{R}^{n+1,l}\left(\mathbf{X}^{n+1,l}\right) = \left(\mathbf{R}_{o}^{n+1,l}, \mathbf{R}_{w}^{n+1,l}, \mathbf{R}_{p}^{n+1,l}, \mathbf{R}_{q}^{n+1,l}\right)^{T} = 0, \quad (18)$$

where X is the array of primary variables, l is the iterating step, and n is the time step.

To solve the above fully implicit discrete equations, the Newton-Raphson method is employed due to its simple formula in programming and fast convergence.

With the above methodology, we can obtain the transient pressure of wells to investigate the influence of non-Newtonian behavior on the transient pressure behavior in viscoelastic polymer flooding systems.

3. Results and Discussion

Firstly, we introduced type curves of the transient pressure response for a falloff test in a viscoelastic polymer flooding system. Then, we compared our model with a model that ignores the influence of the shear thickening behavior. After that, we crafted four scenarios to analyze the influence of shear thickening behavior on the pressure transient response (i.e., near-wellbore damage, polymer injection concentration, injection rate, and permeability).

3.1. Type Curve. Figure 4(a) shows the type curve computed by our model, which considers the influence of the shear thickening behavior and shear thinning behavior of the partially hydrolyzed polyacrylamide (HPAM) solution. The type curve is split into five flow regimes. The first one is the flow regime of wellbore storage (I); the flow regime of near-wellbore damage (II) is significantly influenced by the shear thickening behavior of the HPAM solution. In the flow regime of near-wellbore damage, the pressure and pressure derivative computed by our model are obviously larger than those computed by the model only considering the shear thinning behavior of the HPAM solution, as shown in Figure 4(b). This phenomenon is generated from the increase of the aqueous phase viscosity near the wellbore due to shear thickening behavior of the HPAM solution. Then, the duration of the first radial flow regime (III) is ruled by the range of high concentrate polymer solution due to polymer injection. After that, the flow regime of the transitional zone (IV) is dependent on the concentration gradients generated from polymer injection. Subsequently, the system radial flow regime (V) is dominated by the original fluids in the oil field. The pressure derivative of the system radial flow regime is much smaller than that of the first radial flow regime because the fluid viscosity of the near-well zone increases due to polymer injection.

3.2. Shear Thickening Behavior. To analyze the impact of shear thickening behavior on the pressure transient response of polymer injection wells during falloff tests, four parameters are analyzed. Considering that the influence of shear thickening behavior concentrates on the flow regime of near-wellbore damage, we investigated the impact of the shear thickening behavior on the pressure transient response with different skin factors. Given that the polymer concentration and shear rate have great influences on the polymer rheology (Figure 2), we also analyzed the influence of the shear thickening behavior with different polymer injection concentrations, injection rates, and permeabilities. In these scenarios, a polymer injection well is situated in a 6000 m × 6000 m × 10 m reservoir model with PEBI mesh and regular Cartesian grid. Considering the computing accuracy and computational time, we designate that the radius of each wellbore grid (the minimum PEBI mesh) is 1.24 m, and the size of Cartesian grid is 50 m × 50 m × 10 m. The minimum time step size at the beginning of polymer injection or shut-in is 0.1162 s, and then the time step size exponentially increases to 17117 s. Polymer injection time (t_1) is 374.5 d, and shut-in time (t_2) of the polymer injection well is 51 d

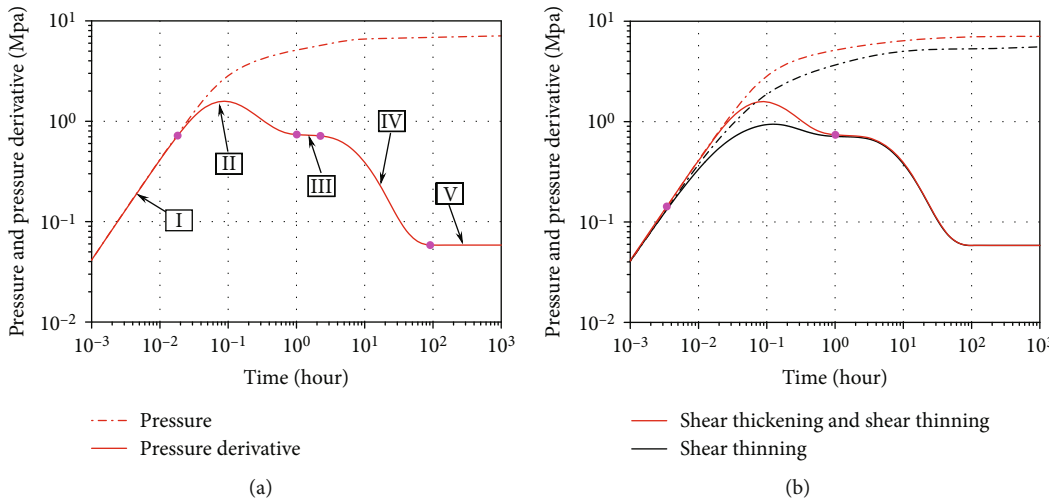

Figure 4: Pressure curves of our model and a model ignoring the influence of the shear thickening behavior. (a) Pressure and pressure derivative curves computed by our model. (b) Pressure curves of our model and a model ignoring the influence of the shear thickening behavior.

Table 2: The basic parameters of the reservoir.

Parameters	Values
Initial reservoir pressure, MPa	20
Well radius, m	0.07
Wellbore storage constant, m^3/MPa	0.1
Porosity, fraction	0.3
Rock compressibility, MPa^{-1}	0.001
Initial water saturation, fraction	0.65
Initial oil saturation, fraction	0.35
Oil viscosity, mPa·s	7.41
Oil compressibility, MPa^{-1}	0.001
Oil volume factor, m^3/m^3	1
Water compressibility, MPa^{-1}	0.0002
Water volume factor, m^3/m^3	1
Initial polymer concentration, kg/m^3	0
Saturated adsorbed concentration of polymer, kg/m^3	0.00005
Constant parameter (b_p), unitless	2.27
Maximum permeability reduction factor, unitless	1.84

during a falloff test. The input parameters are listed in Table 1 and Table 2. The relative permeability curves are illustrated in Figure 5.

To illustrate the difference between viscoelastic polymer and viscous polymer during polymer injection, we also draw the viscosity distribution around the polymer injection well when polymer injection time is 18.38 h. The polymer injection rate is 100 m^3/d, the permeability (K) is 1D, and the polymer injection concentration (C_p) is 1 kg/m^3. As shown in Figure 6, the viscosity of viscoelastic polymer is significantly larger than that of viscous polymer in the near-wellbore region.

3.2.1. Near-Wellbore Damage. To research the influence of shear thickening behavior on the pressure transient response

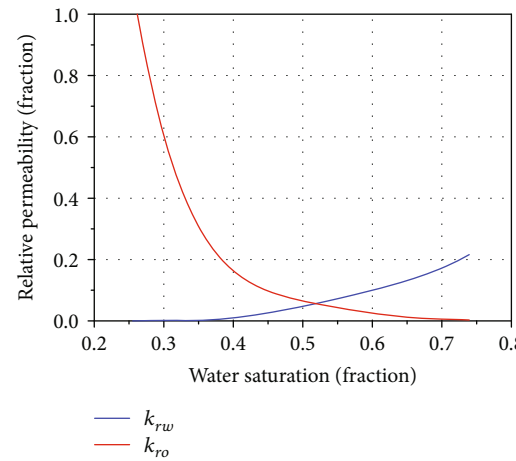

Figure 5: The relative permeability curves.

when degrees of near-wellbore damage are different, our model and the model that ignores the influence of shear thickening behavior are employed to compute the pressure and pressure derivatives with different skin factors (S). In this scenario, the injection rate of the tested well (q) prior to shut-in is 100 m^3/d. The permeability (K) is 1D, and the polymer injection concentration (C_p) is 1 kg/m^3. As illustrated in Figure 7, in the flow regime of near-wellbore damage, the pressure derivative computed by our model is always larger than that computed by the model that ignores the shear thickening behavior when the degree of near-wellbore damage changes. The duration of the flow regime of the near-wellbore damage keeps constant when considering the effect of the shear thickening behavior. However, the pressure derivative increases, and duration expands in the flow regime of near-wellbore damage as the skin factor increases. Therefore, the effect of the shear thickening behavior on the pressure transient response cannot be offset by changing the skin factor in well test interpretation.

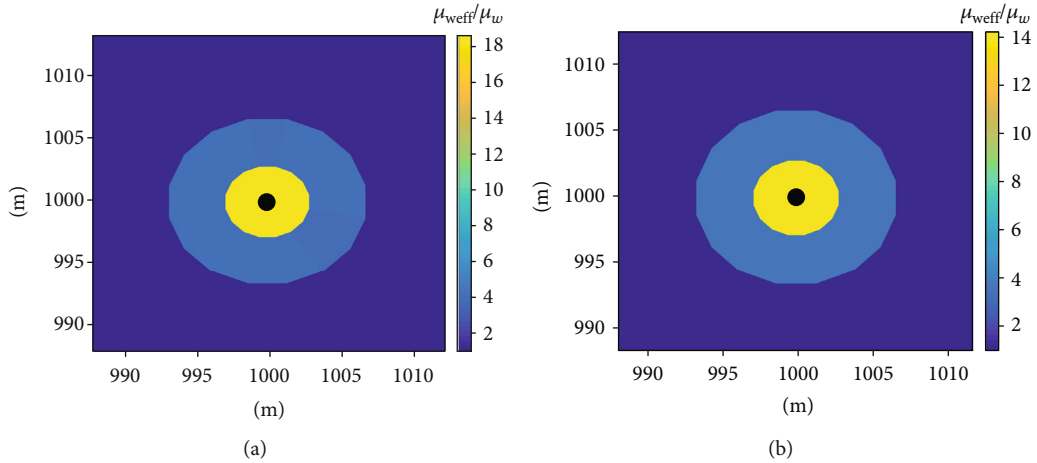

Figure 6: The viscosity distribution around the polymer injection well. (a) The viscosity distribution around the polymer injection well of viscoelastic polymer. (b) The viscosity distribution around the polymer injection well of viscous polymer.

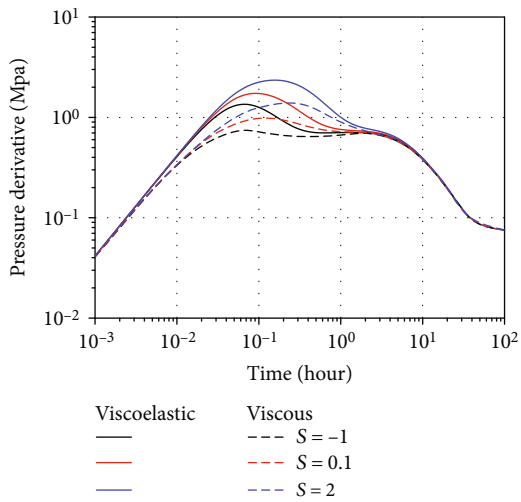

Figure 7: Effect of shear thickening behavior on pressure derivative with different skin factors during falloff tests. (S is the skin factor to represent the degree of the near-wellbore damage. Pressure derivative computed by our model and the model that ignores the shear thickening behavior of the HPAM solution. The solid line is the pressure derivative computed by our model. The dash line is the pressure derivative computed by the model that ignores the shear thickening behavior.)

3.2.2. Polymer Injection Concentration. Given that shear thickening behavior is closely related to polymer concentration, we analyzed the influence of shear thickening behavior on the pressure transient behavior with different polymer injection concentrations. Our model and the model that neglects the influence of shear thickening behavior are applied to compute the pressure transient response with different polymer injection concentrations (C_p). In this scenario, the injection rate of the tested well (q) prior to shut-in is 100 m^3/d. The permeability (K) is 1D, and the skin factor (S) is 0.1. Figure 8 illustrates that the duration of the flow regime affected by the shear thickening behavior increases when the polymer injection concentration increases.

3.2.3. Injection Rate. Since polymer viscosity is a function of the shear rate, the impact of shear thickening behavior on the pressure transient behavior with different injection rates (q) is investigated. In this scenario, the polymer injection concentration (C_p) is 1 kg/m^3, the permeability (K) is 1D, and the skin factor (S) is 0.1. During the flow regime of near-wellbore damage, the influence of the shear thickening behavior on the pressure derivative is more significant when the injection rate grows, as shown in Figure 9.

3.2.4. Permeability. Because the shear rate partly depends on the permeability, we also analyzed the influence of shear thickening behavior on the pressure transient behavior with different permeabilities. Our model and the model that neglects the influence of shear thickening behavior are applied to compute the pressure derivatives with different permeabilities (K). The polymer injection concentration (C_p) is 1 kg/m^3. The injection rate of the tested well (q) prior to shut-in is 100 m^3/d, and the skin factor (S) is 0.1. In the flow regime of near-wellbore damage, the influence of the shear thickening on the pressure derivative is more obvious when the permeability increases, as shown in Figure 10.

4. Field Application

An appropriate model for history matching is the key to attain satisfactory interpretation results for a well test on the basis of geologic information and features of the type curve. However, the shear thickening behavior of viscoelastic polymers was usually ignored by researchers. Now, it has been demonstrated that the shear thickening behavior of viscoelastic polymer solutions cannot be ignored in pressure transient analysis. To validate the accuracy and practicability of our model in viscoelastic polymer flooding systems, we interpreted the transient pressure data obtained from a tested injection well in a reservoir with HPAM polymer flooding, in which we employed our model and the mode that ignores the shear thickening behavior.

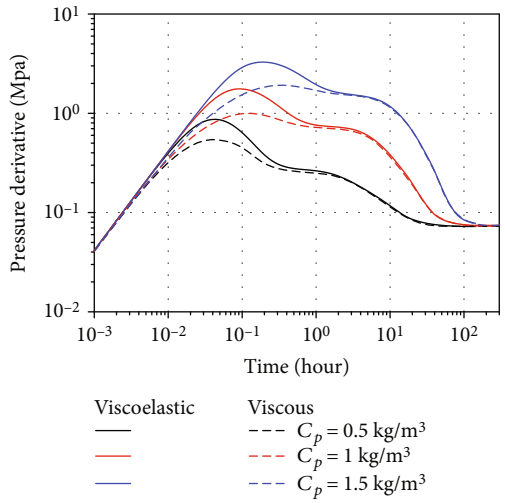

Figure 8: Impact of shear thickening behavior on pressure derivative with different polymer injection concentrations during falloff tests. The solid line is the pressure derivative computed by our model. The dash line is the pressure derivative computed by the model that ignores the shear thickening behavior.

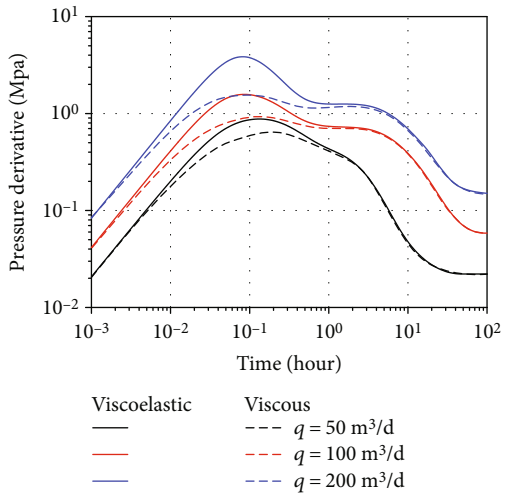

Figure 9: Effect of shear thickening behavior on pressure derivative with different injection rates during falloff tests. The solid line is the pressure derivative computed by our model. The dash line is the pressure derivative computed by the model that ignores the shear thickening behavior of the HPAM solution.

4.1. Basic Information of a Falloff Test in a Reservoir with HPAM Polymer Flooding. The basic parameters of a falloff test in a reservoir with HPAM polymer flooding are illustrated in Table 3. The relative permeability curves are shown in Figure 5. The input parameters of the HPAM solution are exhibited in Tables 1 and 2. The polymer flooding started in October 2014. The date of falloff test is October 14, 2015. The injection time prior to shut-in is 177 d. The effective shut-in time is 71.46 hr.

4.2. Well Test Interpretation. In this section, our model and the model that ignores the influence of shear thickening

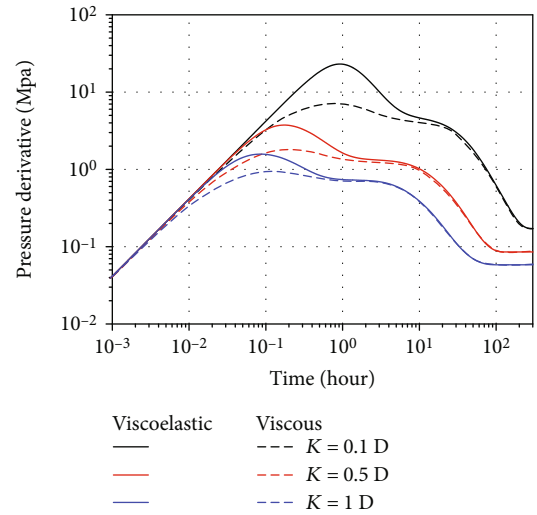

Figure 10: Effect of shear thickening behavior on pressure derivative with different permeabilities during falloff tests. The solid line is the pressure derivative computed by our model. The dash line is the pressure derivative computed by the model that ignores the shear thickening behavior.

Table 3: The basic parameters of a field case.

Parameters	Values
Porosity, fraction	0.174
Rock compressibility, MPa^{-1}	1.46×10^{-3}
Thickness, m	13
Initial water saturation, fraction	0.649
Water viscosity, mPa·s	0.99
Oil viscosity, mPa·s	7.41
Water compressibility, MPa^{-1}	1.5×10^{-4}
Oil compressibility, MPa^{-1}	2×10^{-3}
Water volume factor, m^3/m^3	1.001
Oil volume factor, m^3/m^3	1.174
Well radius, m	0.07
Injection rate of tested well, m^3/d	60
Polymer injection concentration, kg/m^3	0.503
Polymer concentration of adjacent production well, kg/m^3	0

behavior are employed to interpret the transient pressure data derived from a falloff test. We outline our matching methodology in the following procedure.

Step 1. Input the parameters listed in Section 4.1 and transient pressure data from the tested well into the computation procedure on the basis of our model.

Step 2. To reduce the matching time, the limitations of certain unknown parameters can be set according to the geologic and dynamic information of the field case.

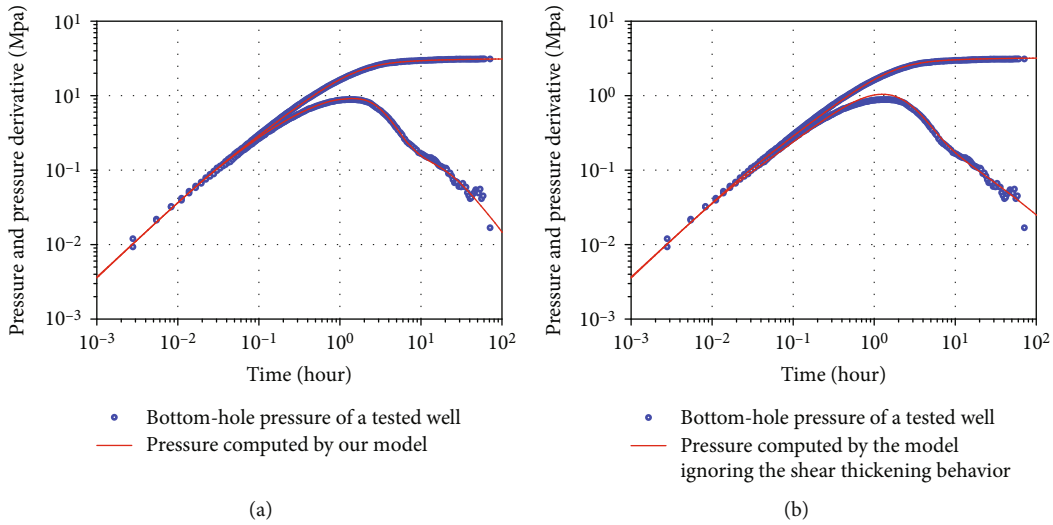

Figure 11: History matching results computed by our model and the model that ignores the influence of shear thickening behavior. (a) History matching using our model that considers the shear thickening behavior and shear thinning behavior of the HPAM solution. (b) History matching using the model that ignores the influence of shear thickening behavior.

Table 4: Interpretation results.

Interpreting parameters	Values interpreted by our model	Values interpreted by the model ignoring shear thickening
Wellbore storage constant, m^3/MPa	0.917	0.917
Skin factor, unitless	-0.41	2.06
Permeability, D	0.42	0.42

Step 3. Regulate the unknown variables based on the results obtained from the above discussion results. More specifically, the features of the flow regimes of the near-wellbore damage and transitional zone are significant and identifiable, which can be used to assist with parameters adjustment in history matching.

As illustrated in Figure 11(a), the pressure and pressure derivative computed by our model agree well with the transient pressure data obtained from the tested well, which validates the applicability and accuracy of our model. The interpretation results are listed in Table 4. However, the pressure curves computed by the model ignoring the shear thickening behavior match the pressure data poorly in the flow regime of near-wellbore damage, as shown in Figure 11(b). Furthermore, Table 4 shows that the skin factor interpreted by the model ignoring shear thickening is obviously larger than that interpreted by our model, which can lead to a false impression on the near-wellbore damage.

5. Conclusions

Although viscoelastic polymer solutions show shear thickening behavior in the near-wellbore region due to high shear rate, the effect of shear thickening behavior on the pressure transient response was commonly ignored in well test interpretation. To better characterize the oilfields with pressure transient analysis in viscoelastic polymer flooding systems, we developed a numerical mode that takes into account both shear thickening behavior and shear thinning behavior. The finite volume method and fully implicit Newton-Raphson method were employed to solve the model in a hybrid grid system. The investigation of our model led to the following conclusions:

(1) The influence of shear thickening behavior on pressure derivative is different from that of near-wellbore damage. In the flow regime of near-wellbore damage, the pressure derivative computed by our model is obviously larger than that computed by the model ignoring shear thickening behavior. The duration of the flow regime of the near-wellbore damage remains constant when considering the effect of the shear thickening behavior

(2) The flow regime of near-wellbore damage lasts longer when the polymer injection concentration increases. The influence of the shear thickening on the pressure derivative is more significant when the injection rate or permeability increases

(3) The skin factor interpreted by the model that ignores the effect of shear thickening behavior is much larger than that interpreted by our model, which can lead to false impression on the degree of near-wellbore damage

Nomenclature

ϕ: Rock porosity, fraction
α: Oil or water phase
o: Oil phase
w: Water phase
S_α: Oil or water saturation, fraction

b_α: Reciprocal of the oil/water formation volume factor, m^3/m^3
p_α: Oil/water pressure in reservoir, MPa
v_α: Velocity oil/water phase in porous media, m^3/s
Q_α: Well flux of phase α, m^3/d
f_p: Ratio of the accessible pore volume to the pore volume of reservoir rocks, fraction
$C^\wedge_p$: Adsorbed concentration of the polymer on the rock surface, kg/m^3
C_p: Polymer concentration in the aqueous phase, kg/m^3
K: Absolute permeability of reservoir, D
$k_{r\alpha}$: Relative permeability of phase α, fraction
μ_o: Viscosity of oil phase, mPa·s
μ_{weff}: Effective viscosity of aqueous phase in polymer flooding systems, mPa·s
R_k: Permeability reduction factor of the aqueous phase, unitless
$C^\wedge_{p\ max}$: Saturated adsorbed concentration of polymer, kg/m^3
b_p: Constant parameter, unitless
$R_{k\ max}$: Maximum permeability reduction factor, unitless
Q_s: Total well flux of oil and water, m^3/d
λ_α: Ratio of relative permeability to viscosity for phase α
h: Thickness of each layer, m
r_e: Equivalent radius in well flux equation, m
r_w: Wellbore radius, m
S: Skin factor, unitless
p_{wf}: Bottom-hole pressure, MPa
C: Wellbore storage factor, m^3/MPa
t: Time, s
μ_w: Water viscosity, mPa·s
γ: The shear rate, s^{-1}
μ_p^0: The zero shear viscosity of polymer solution, mPa·s
n_1: Empirical constant, unitless
n_2: Empirical constant, unitless
λ_2: Empirical constant, unitless
λ_1: Model parameter, unitless
μ_{max}: Model parameter, mPa·s
τ_r: Model parameter, unitless
β_1: Model parameter, unitless
β_2: Model parameter, unitless
A_{p1}: Model parameter, unitless
A_{p2}: Model parameter, unitless
τ_0: Model parameter, unitless
τ_1: Model parameter, unitless
C_{sep}: Effective salinity in aqueous phase, kg/m^3
sp: Model parameter, unitless
A_1: Model parameter, unitless
A_2: Model parameter, unitless
A_3: Model parameter, unitless
C': Model parameter, unitless
n: Model parameter, unitless
div: Divergence operator
grad: Gradient operator
$\mathbf{q}$: Array of discrete fluxes, m^3/d
f: Face
c: Cell
$\mathbf{p}$: Array of discrete pressures
$\mathbf{T}$: Array of discrete transmissibilities across faces
c: Cell in the grid system
f: Face in the grid system
n: Time step
l: Iterating step
$\mathbf{V}$: Array of grid volume
$\mathbf{R}_\alpha$: Array of discrete form of conservation equation of phase α
$\mathbf{R}_p$: Array of discrete form of conservation equation of polymer
$\mathbf{R}_q$: Array of discrete form of well equation of phase α
$\mathbf{X}$: Array of primary variables
$\boldsymbol{\phi}$: Array of rock porosity
$\mathbf{S}_\alpha$: Array of oil or water saturation
$\mathbf{b}_\alpha$: Array of inverse formation-volume factor of oil/water
$\mathbf{v}_\alpha$: Array of oil or water velocity in porous media
$\mathbf{Q}_\alpha$: Array of well flux of phase α
$\mathbf{C}^\wedge_p$: Array of adsorbed concentration of the polymer on the rock surface
$\mathbf{C}_p$: Array of polymer concentration in the aqueous phase
$\boldsymbol{\lambda}_\alpha$: Array of ratio of relative permeability to viscosity for phase α
$\mathbf{p}_\alpha$: Array of oil or water pressure in reservoir
$\mathbf{p}_{wf}$: Array of bottom-hole pressure
$\mathbf{Q}_s$: Array of total well flux of oil and water
q: Rate of the testing injector, m^3/d
t_1: Polymer injection time for the tested well, d
t_2: Shut-in time for the tested well, d.

Data Availability

The data used to support the findings of this study are available from the corresponding author upon request.

Conflicts of Interest

The authors declare no conflicts of interest.

Acknowledgments

We gratefully acknowledge the financial support from the National Science and Technology Major Projects (No. 2016ZX05025-003, No. 2016ZX05055004), Natural Science Basic Research Program of Shaanxi (No. 2020JQ-781), and Scientific Research Program Funded by Shaanxi Provincial Education Department (No. 20JS117).

References

[1] D. J. Pye, "Improved secondary recovery by control of water mobility," *Journal of Petroleum Technology*, vol. 16, no. 8, pp. 911–916, 1964.

[2] B. B. Sandiford, "Laboratory and field studies of water floods using polymer solutions to increase oil recoveries," *Journal of Petroleum Technology*, vol. 16, no. 8, pp. 917–922, 1964.

[3] W. B. Gogarty, "Mobility control with polymer solutions," *Society of Petroleum Engineers Journal*, vol. 7, no. 2, pp. 161–173, 1967.

[4] D. C. Standnes and I. Skjevrak, "Literature review of implemented polymer field projects," *Journal of Petroleum Science and Engineering*, vol. 122, pp. 761–775, 2014.

[5] L. W. Lake, R. Johns, B. Rossen, and G. Pope, *Fundamentals of Enhanced Oil Recovery*, Society of Petroleum Engineers, 2014.

[6] A. Al-Bemani and I. Ershaghi, "Two-phase flow interporosity effects on pressure transient test response in naturally fractured reservoirs," in *SPE Annual Technical Conference and Exhibition*, Dallas, Texas, 1991.

[7] G. M. Warren, "Numerical solutions for pressure transient analysis," in *SPE Gas Technology Symposium*, Calgary, Alberta, Canada, 1993.

[8] X. W. Liao and L. M. Liu, "Three-dimensional two-phase-flow numerical well testing model," *Journal-University of Petroleum China Natural Science Edition*, pp. 42–44, 2003.

[9] Z. P. Xiang, L. H. Zhang, and H. Chen, "Influence of the relative permeability curve on numerical well test curve of oil-water-phase flow," *Journal of Southwest Petroleum University*, 2007.

[10] Y. Wu, L. Cheng, S. Fang, S. Huang, and P. Jia, "A green element method-based discrete fracture model for simulation of the transient flow in heterogeneous fractured porous media," *Advances in Water Resources*, vol. 136, article 103489, 2020.

[11] Y. He, J. Qin, S. Cheng, and J. Chen, "Estimation of fracture production and water breakthrough locations of multi-stage fractured horizontal wells combining pressure-transient analysis and electrical resistance tomography," *Journal of Petroleum Science and Engineering*, vol. 194, p. 107479, 2020.

[12] Y. Wu, L. Cheng, S. Fang, J. E. Killough, S. Huang, and P. Jia, "A novel edge-based green element method for simulating fluid flow in unconventional reservoirs with discrete fractures," *SPE Journal*, vol. 25, no. 2, pp. 842–866, 2020.

[13] O. O. Eleri and J. R. Ursin, "Physical aspects of formation damage in linear flooding experiments," in *SPE Formation Damage Control Symposium*, Lafayette, LA, 1992.

[14] C. Roque, G. Chauveteau, M. Renard, G. Thibault, M. Bouteca, and J. Rochon, "Mechanisms of formation damage by retention of particles suspended in injection water," in *SPE European Formation Damage Conference*, The Hague, Netherlands, 1995.

[15] H. Liu, "Experimental research on formation damage by cold water injection in Beixiaohu oilfield," *Journal of The University of Petroleum, China*, vol. 5, 2001.

[16] I. M. Mohamed, G. I. Block, O. A. Abou-Sayed, S. M. Elkatatny, and A. S. Abou-Sayed, "Flow rate-dependent skin in water disposal injection well," *Journal of Energy Resources Technology*, vol. 138, no. 5, 2016.

[17] J. Li, X. Li, X. Wang et al., "Water distribution characteristic and effect on methane adsorption capacity in shale clay," *International Journal of Coal Geology*, vol. 159, pp. 135–154, 2016.

[18] F. Civan, *Reservoir Formation Damage*, Gulf Professional Publishing, Boston, 3rd edition, 2016.

[19] J. Li, X. Li, K. Wu et al., "Water sorption and distribution characteristics in clay and shale: effect of surface force," *Energy & Fuels*, vol. 30, no. 11, pp. 8863–8874, 2016.

[20] K. Prempeh, L. Chequer, A. Badalyan, and P. Bedrikovetsky, "Effects of Kaolinite on Fines Migration and Formation Damage," in *SPE International Conference and Exhibition on Formation Damage Control*, Lafayette, LA, USA, 2020.

[21] D. M. Meter and R. B. Bird, "Tube flow of non-Newtonian polymer solutions: PART I. Laminar flow and rheological models," *AICHE Journal*, vol. 10, no. 6, pp. 878–881, 1964.

[22] W. B. Gogarty, G. L. Levy, and V. G. Fox, "Viscoelastic effects in polymer flow through porous media," in *Fall Meeting of the Society of Petroleum Engineers of AIME*, San Antonio, Texas, 1972.

[23] G. Chauveteau, "Rodlike polymer solution flow through fine pores: influence of pore size on rheological behavior," *Journal of Rheology*, vol. 26, no. 2, pp. 111–142, 1982.

[24] R. S. Seright, J. M. Seheult, and T. Talashek, "Injectivity characteristics of EOR polymers," in *SPE Annual Technical Conference and Exhibition*, Denver, CO, USA, 2008.

[25] F. W. Smith, "The behavior of partially hydrolyzed polyacrylamide solutions in porous media," *Journal of Petroleum Technology*, vol. 22, no. 2, pp. 148–156, 1970.

[26] R. R. Jennings, J. H. Rogers, and T. J. West, "Factors influencing mobility control by polymer solutions," *Journal of Petroleum Technology*, vol. 23, no. 3, pp. 391–401, 1971.

[27] J. Heemskerk, R. Rosmalen, R. Janssen-van, R. J. Holtslag, and D. Teeuw, "Quantification of viscoelastic effects of polyacrylamide solutions," in *SPE Enhanced Oil Recovery Symposium*, Tulsa, Oklahoma, 1984.

[28] Y. Masuda, K. C. Tang, M. Miyazawa, and S. Tanaka, "1D simulation of polymer flooding including the viscoelastic effect of polymer solution," *SPE Reservoir Engineering*, vol. 7, no. 2, pp. 247–252, 1992.

[29] H. K. Van Poollen and J. R. Jargon, "Steady-state and unsteady-state flow of non~Newtonian fluids through porous media," *Society of Petroleum Engineers Journal*, vol. 9, no. 1, pp. 80–88, 1969.

[30] C. U. Ikoku and H. J. Ramey Jr., "Transient flow of non-Newtonian power-law fluids in porous media," *Society of Petroleum Engineers Journal*, vol. 19, no. 3, pp. 164–174, 1979.

[31] A. S. Odeh and H. T. Yang, "Flow of non-Newtonian power-law fluids through porous media," *Society of Petroleum Engineers Journal*, vol. 19, no. 3, pp. 155–163, 1979.

[32] O. Lund and C. U. Ikoku, "Pressure transient behavior of non-Newtonian/Newtonian fluid composite reservoirs," *Society of Petroleum Engineers Journal*, vol. 21, no. 2, pp. 271–280, 1981.

[33] J. A. Murtha and T. Ertekin, "Numerical simulation of power-law fluid flow in a vertically fractured reservoir," in *SPE Annual Technical Conference and Exhibition*, San Francisco, California, 1983.

[34] S. Vongvuthipornchai and R. Raghavan, "Pressure falloff behavior in vertically fractured wells: non-Newtonian power-law fluids," *SPE Formation Evaluation*, vol. 2, no. 4, pp. 573–589, 1987.

[35] H. Mahani, T. G. Sorop, P. J. Van den Hoek, A. D. Brooks, and M. Zwaan, "Injection fall-off analysis of polymer flooding EOR," in *SPE Reservoir Characterisation and Simulation Conference and Exhibition*, Abu Dhabi, UAE, 2011.

[36] M. M. Kamal, C. Tian, and F. Suleen, "Pressure transient analysis of polymer flooding with coexistence of non-Newtonian and Newtonian fluids," *SPE Reservoir Evaluation & Engineering*, vol. 22, no. 3, pp. 1172–1184, 2019.

[37] D. Zhang and J. Yao, "Sensitivity of testing parameters of a two phase well with polymer flooding," *Chinese Journal of Computational Physics*, vol. 23, no. 4, p. 425, 2006.

[38] J. Zhichun, L. Daolun, Y. Jinghai, X. Zhenggang, and L. Detang, "Numerical well test analysis for polymer flooding

considering the non- Newtonian behavior," *Journal of Chemistry*, vol. 2015, Article ID 107625, 10 pages, 2015.

[39] W. Yang, H. Yin, H. Zhong, and S. Y. Meng, "Well test analysis of viscoelastic polymer solution," *Journal of Hydrodynamics*, vol. 22, no. S1, pp. 366–369, 2010.

[40] Q. Xie, J. Xu, and M. Chen, "Unsteady pressure dynamics of polymer flooding reservoirs considering concentration changes," *Chemistry and Technology of Fuels and Oils*, vol. 56, no. 3, pp. 481–491, 2020.

[41] Y. Ma and M. W. McClure, "The effect of polymer rheology and induced fracturing on injectivity and pressure-transient behavior," *SPE Reservoir Evaluation & Engineering*, vol. 20, no. 2, pp. 394–402, 2017.

[42] J. Hou, Z. Q. Li, Y. D. Wang, and Y. M. Chen, "Numerical simulation of polymer flooding with dispersion and adsorption," *Chinese Journal of Computational Physics*, vol. 20, no. 3, pp. 239–244, 2003.

[43] M. Delshad, D. H. Kim, O. A. Magbagbeola, C. Huh, G. A. Pope, and F. Tarahhom, "Mechanistic interpretation and utilization of viscoelastic behavior of polymer solutions for improved polymer-flood efficiency," in *SPE Symposium on Improved Oil Recovery*, Tulsa, Oklahoma, USA, 2008.

[44] X. Wang and G. Zhao, "Shear rate of power-law fluid through porous media," *Xinjiang Petroleum Geology*, vol. 19, no. 4, p. 312, 1998.

[45] X. Wang, "Determination of the main parameters in the numerical simulation of polymer flooding," *Petroleum Exploration and Development*, vol. 3, 1990.

[46] W. J. Cannella, C. Huh, and R. S. Seright, "Prediction of xanthan rheology in porous media," in *SPE Annual Technical Conference and Exhibition*, Houston, Texas, 1988.

[47] R. J. LeVeque, *Finite volume methods for hyperbolic problems. Vol. 31*, Cambridge university press, 2002.

[48] K. A. Lie, *An Introduction to Reservoir Simulation Using MATLAB/GNU Octave: User Guide for the MATLAB Reservoir Simulation Toolbox (MRST)*, Cambridge University Press, 2019.

[49] J. Zhang, S. Cheng, S. Di, Z. Gao, R. Yang, and P. Cao, "A two-phase numerical model of well test analysis to characterize formation damage in near-well regions of injection wells," *Geofluids*, vol. 2021, Article ID 6693965, 15 pages, 2021.